RSC Advances

PAPER

View Article Online
View Journal | View Issue

Cite this: *RSC Adv.*, 2018, **8**, 454

Study on the corrosion behavior of steel Q315NS heat-affected zone in a HCl solution using electrochemical noise

S. Q. Zhang,[a] H. Y. Zhao,[a] F. Y. Shu,*[a] G. D. Wang,[ab] B. Liu[c] and B. S. Xu[d]

Received 14th November 2017
Accepted 12th December 2017

DOI: 10.1039/c7ra12404j

rsc.li/rsc-advances

The microstructure and corrosion behavior of a base metal (BM) and heat-affected zone (HAZ) of Q315NS steel in 0.1 mol L^{-1} HCl solution at 60 °C were investigated with a thermal simulation technique, surface observation and electrochemical measurements. The transient characteristics, as well as the power spectral density (PSD) and wavelet transform, had been employed to analyze the electrochemical noise (EN) data. It was revealed that the microstructure of BM, the fine grained region (FGHAZ) and the inter critical region (ICHAZ) mainly consisted of ferrite and pearlite, while the coarse grained region (CGHAZ) mainly consisted of granular bainite. The corrosion processes of BM, FGHAZ and ICHAZ were similar and characterized by two stages. The first stage involved the metastable pitting process and the second stage corresponded to the pitting corrosion. On the CGHAZ electrode, metastable pitting occurred in the initial corrosion stage and then the corrosion process turned into uniform corrosion. With increasing corrosion time, the corrosion strength of all electrodes decreased significantly at first and then remained constant. The corrosion rate of CGHAZ was slightly lower than the other electrodes in the second corrosion stage, and there was no obvious difference in corrosion rate among BM, FGHAZ and ICHAZ.

1 Introduction

Metallic components in petrochemical and power industries are seriously corroded when corrosive gases (SO_3, HCl, NO_2, *etc.*) are cooled and converted to condensed acids on the metal surface, which is defined as dew point corrosion (DPC).[1] Corrosion resistant steel Q315NS is much more appropriate for components serving in a DPC environment due to its excellent DPC resistance and low cost. Q315NS is produced by appropriate alloy design, in which Cu and Sb have a significant impact on improving the corrosion resistance.[2–5] Cu is capable of enhancing the activity of the cathode, which will promote the passivation of the anode under certain conditions. Thereby the corrosion rate reduces due to the passivation of the anode. In addition, the enrichment of Cu in the corrosion product is able to greatly improve the corrosion protection performance. The Cu_2S in the corrosion product can simultaneously prevent the corrosion process in the case of an appropriate amount Sb being contained in the steel. The Sb in steel can increase the electrode potential to inhibit the corrosion process, and the dense Cu_2Sb film formed on the surface of the electrode also has an excellent corrosion inhibition performance. However, excessive Sb will reduce the processability of Q315NS because it is in the form of an impurity in the steel.[6]

Q315NS is gradually being used for producing metallic components in electric, metallurgy and petrochemical equipment, such as economizers, air preheaters, chimneys, and furnace walls, *etc.*[7,8] Welding is an essential procedure in the manufacture of metallic components and plays an important role on the microstructure evolution of the heat affected zone (HAZ) which is related to the corrosion process of the HAZ.[9–13] The corrosion behavior of the HAZ of Q315NS in a DPC environment is very important to the reliability and safety of equipment which is made from Q315NS. Therefore, it is essential to investigate the corrosion behavior of the HAZ of Q315NS, which can provide an important foundation for optimizing the welding parameters of Q315NS.

H_2SO_4 corrosion and HCl corrosion are most common in DPC. The corrosion behavior of a base metal (BM) and the HAZ of Q315NS in a H_2SO_4 solution has been investigated.[14] However, the corrosion behavior of Q315NS and the corresponding HAZ in HCl solution is lacking. In this paper, the corrosion behavior of the BM and HAZ of Q315NS in HCl solution was investigated. The electrochemical noise (EN) measurements of the Q315NS and the corresponding HAZ were performed in a 0.1 mol L^{-1} HCl solution at 60 °C, in coordination with potentiodynamic polarization, EIS and surface

---

[a] *Shandong Provincial Key Lab of Special Welding Technology, Harbin Institute of Technology, Harbin 150001, China. E-mail: shufengyuanhit@163.com*

[b] *State Key Laboratory of Rolling and Automation, Northeastern University, Shenyang 110819, China*

[c] *School of Materials Science and Engineering, Jiangsu University of Science and Technology, Zhenjiang, 212003, China*

[d] *National Key Laboratory for Remanufacturing, Academy of Armoured Forces Engineering, Beijing 100072, China*

observation. The time domain analysis, frequency domain analysis, wavelet transform and noise resistance have been used to interpret the EN data. The HAZ specimens were prepared using the welding thermal simulation method, which is capable of preparing simulated HAZ specimens with a homogeneous microstructure. The aim of this paper is to survey the corrosion processes of the BM and HAZ of Q315NS steel and to reveal the influence of welding thermal cycles on the corrosion behaviors of Q315NS in a 0.1 mol L^{-1} HCL solution.

2 Experimental

2.1 Welding thermal simulation experiment

The Q315NS steel was used as the BM for the welding thermal simulation processing, which was carried out in a thermal-mechanical physical simulation Gleeble 3800 (Dynamic Systems Inc., USA). The chemical composition of the Q315NS steel, which was determined by the chemical analysis method, is shown in Table 1. The cuboid specimens, with the dimensions of 10 mm × 10 mm × 55 mm, were prepared for the welding thermal simulation experiments. The simulated specimens were heated to peak temperature at the rate of 150 °C s^{-1}, held for 1 s at peak temperature and then cooled down to 300 °C within the given time. The HAZ specimens, including the coarse grained region (CGHAZ), the fine grained region (FGHAZ) and the inter critical region (ICHAZ) were simulated.

In general, the microstructure of the HAZ for steel mainly depends on the peak temperature and cooling rate. Complete austenite transformation occurs in CGHAZ when the peak temperature is significantly higher than the end temperature of austenite transformation (A_{C3}). Complete austenite transformation also occurs in FGHAZ, though the peak temperature is slightly above the A_{C3}. Incomplete austenite transformation occurs in ICHAZ because the specific peak temperature is between A_{C3} and the start temperature of austenite transformation (A_{C1}).[15–17] The A_{C3} and A_{C1} were 909 °C and 721 °C respectively, according to the following empirical equation proposed by Andrews:[18]

$$A_{C1} = 732 - 10.7\omega_{Mn} - 3.9\omega_{Ni} + 29\omega_{Si} + 16.7\omega_{Cr} + 290\omega_{As} + 6.38\omega_{W} \quad (1)$$

$$A_{C3} = 910 - 230{\omega_C}^{0.5} - 15.2\omega_{Ni} + 44.7\omega_{Si} + 104\omega_{V} + 31.5\omega_{Mo} + 13.1\omega_{W} \quad (2)$$

where ω is the mass fraction of the elements.

Thus, the peak temperatures of CGHAZ, FGHAZ and ICHAZ were set as 1320 °C, 930 °C and 830 °C, respectively. The heat input of 15 kJ cm^{-1}, which was common in the real welding process, was selected and thus the $T_{8/5}$ (cooling time from 800 °C to 500 °C) was set as 15 s according to the following empirical equation:[19]

$$T_{8/5} = Q^2\delta^2F(0.043 - 4.3 \times 10^{-5} \times T_0)[1/(500 - T_0)^2 - 1/(800 - T_0)^2] \quad (3)$$

where Q refers to the welding heat input, δ is the thickness of the steel plate, F represents the shape factor of the weldment and T_0 stands for the initial temperature of the steel.

After the welding thermal simulation experiments, the middle part of the simulated HAZ specimens were cut down to the size of 10 mm × 10 mm × 6 mm. They were then used as test electrodes in the following electrochemical experiments.

Table 1 Chemical composition of Q315NS

Element	C	Si	Mn	S	P	Ni	Mo	Cu	Sb	Fe
wt%	0.06	0.27	0.87	0.02	0.01	0.11	0.10	0.31	0.09	Bal.

2.2 Electrochemical experiments

Following the electrical connection with the copper wire, the test electrodes were mounted in epoxy resin. All test electrodes for the electrochemical measurements were finished by grinding with 800 grit silicon carbide (SiC) abrasive paper. Fig. 1 shows the schematic diagram of the EN measurement system. The EN measurements were performed at the open circuit potential (OCP) in the Zennium electrochemistry work station equipped with an EPC40 noise probe set (Zahner elektrik GmbH & Co. KG, Germany). Two identical test electrodes including BM and a simulated HAZ of Q315NS were set as the working electrodes and a saturated calomel electrode (SCE) was set as the reference electrode in the EN measurement system. The EN signals were recorded with the step width of 0.049 s for 10 h. The potentiodynamic polarization and EIS measurements were performed in a Zennium electrochemistry work station with the conventional three electrode electrochemical system, in which BM and the simulated HAZ of Q315NS were set as the working

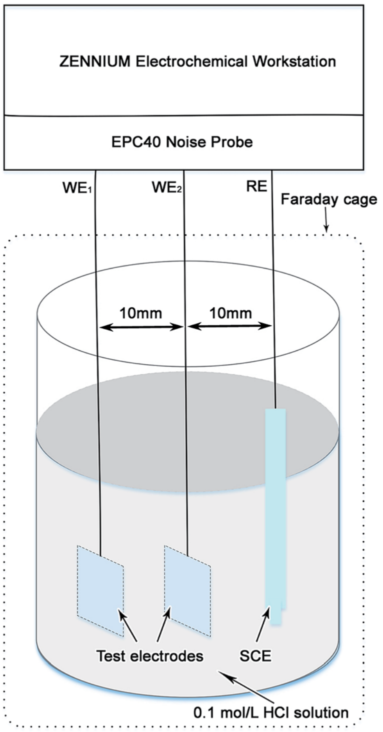

Fig. 1 Schematic diagram of the EN measurement system.

electrodes, a Pt electrode was set as the auxiliary electrode and a SCE was set as the reference electrode. The potentiodynamic polarization curves were measured with the scan rate of 0.5 mV s^{-1}, and the EIS measurements were carried out with the frequency range of 10^{-1}–10^4 Hz. The area of all the working electrodes and the auxiliary electrode in the electrochemical measurements was 10 mm × 10 mm, and the electrolyte was a 0.1 mol L^{-1} HCl solution which was prepared by dilution of analytical reagent grade 38 wt% HCl with de-ionized water. All the electrochemical measurements were carried out at the temperature of 60 °C.

2.3 Microstructure observation

The BM and simulated HAZ specimens of Q315NS were ground with SiC abrasive paper to 1200 grit and then polished for less than 3 min. All specimens were dried in cool air following ultrasonic cleaning for more than 5 min. The microstructure of the BM and simulated HAZ of Q315NS were observed by Merlin Compact field emission scanning electron microscope (FESEM, ZEISS, Germany) after being etched with an alcohol solution containing 4 vol% HNO_3. In addition, the morphology of the BM and simulated HAZ after 10 h corrosion in 0.1 mol L^{-1} HCl solution were also were observed by FESEM.

3 Results and discussion

3.1 Time domain analysis

The DC drift signals were included in the original EN records owing to the instability of the EN measurement system, which has been confirmed as one of the main reasons for analysis errors.[20,21] Thus, the moving average (MAR) method proposed by Tan[22–24] was used to remove the DC drift before the analysis of the EN records. The transients of EN records have the ability to characterize the corrosion process of electrodes in detail. The EN records of BM and the simulated HAZ electrodes after MAR including electrochemical potential noise (EPN) and electrochemical current noise (ECN) records are shown in Fig. 2 to 5.

In the initial corrosion stage of BM, the feature of sudden drop after slow rise could be found periodically in ECN and EPN as shown in Fig. 2(a). The fluctuation amplitudes of EPN and ECN were about 1 mV and 0.4 mA respectively, and the interval time of these fluctuations was about 100 s. It has been reported that the fluctuations of EPN reflect the charge and discharge of the electrode capacitance and the ECN can be considered as the indication of initiation and extinction of pits.[25] The slow rise of the ECN and EPN corresponded to the initiation process of the pits and the sudden drop of ECN and EPN indicated the extinction of pits (repassivation). The coexistence of the sudden drop and the slow rise in EN records indicated the competition process of pitting and repassivation, which meant that the metastable pitting occurred on the BM electrode surface. At the later corrosion stage (after 1200 s), there was change in the characteristics of the EN records of BM. As shown in Fig. 2(b) to (d), the sudden drop in ECN and EPN disappeared in this stage, which indicated that the repassivation process no longer exists on the electrode. Instead, both the ECN and EPN were dominated by high frequency fluctuations and a number of large fluctuation, which revealed that the corrosion in this stage was mixed controlled by activation control and diffusion control.[26] Generally, anodic dissolution and hydrogen evolution are undertaken on steel. Lots of high frequency fluctuations in ECN records reflected the constant occurrence of pitting, while the large fluctuation might be associated with the evolution of hydrogen. The generation of hydrogen bubbles occurred when hydrogen was adsorbed onto the electrode surface, which prevented the anodic dissolution of the electrode from the corrosive electrolyte. The adsorbed hydrogen bubbles led to the decrease of the anodic dissolution area, which was the cause of the abrupt drop of EN records. The sharp rise of EN records indicated the regression of the anodic dissolution area, which was caused by the desorption of these hydrogen bubbles when they grew up to a certain size. Therefore, the absorption and desorption of hydrogen bubbles caused the periodical transients characterized by sharp and large fluctuations in the EN records.

Fig. 3 shows the EN time records of CGHAZ. In the initial corrosion stage, the fluctuation of EN of CGHAZ showed a similar characteristic as compared with that of BM, as shown in Fig. 3(a). It was indicated that there was no obvious difference between the corrosion process of CGHAZ and BM in the initial corrosion stage. This pattern lasted for about 2100 s, and then

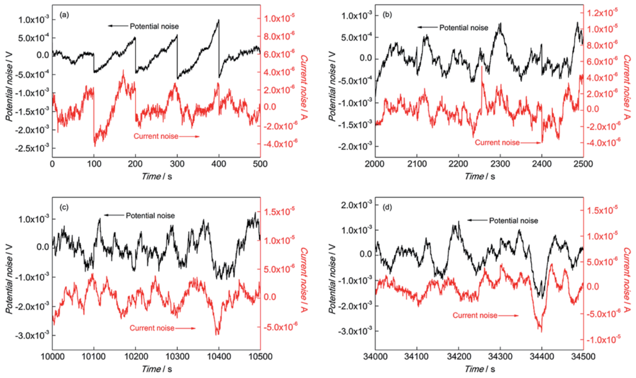

Fig. 2 EN records of BM during (a) 0–500 s, (b) 2000–2500 s, (c) 10 000–10 500 s and (d) 34 000–34 500 s in 0.1 mol L^{-1} HCl solution.

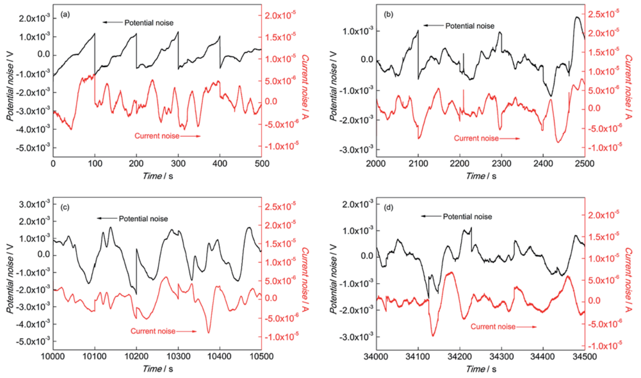

Fig. 3 EN records of CGHAZ during (a) 0–500 s, (b) 2000–2500 s, (c) 10 000–10 500 s and (d) 34 000–34 500 s in 0.1 mol L^{-1} HCl solution.

the fluctuation characteristic changed: large fluctuations dominated the EN records of CGHAZ. It was implied that the corrosion process in this stage was mainly controlled by the absorption and desorption of hydrogen, which was a typical feature of uniform corrosion.[23]

Fig. 4 and 5 show the EN time records of FGHAZ and ICHAZ. It seemed that the pitting corrosion occurred after the metastable pitting, according to the transient characteristics of FGHAZ and ICHAZ, which was similar to BM.

3.2 Noise resistance

The noise resistance (R_n) is an important indicator to corrosion resistance. Generally, $1/R_n$ is proportional to the corrosion rate. R_n can be calculated according to eqn (4) as follows:[27]

$$R_n = \sigma_v/\sigma_i \tag{4}$$

where σ_v and σ_i are standard deviation of EPN and ECN, respectively.

The variations of $1/R_n$ of BM and simulated HAZ electrodes immersed in 0.1 mol L^{-1} HCl solution are shown in Fig. 6. Each value of $1/R_n$ was obtained from calculating EN records of 15 minutes. At the beginning, the $1/R_n$ of BM exhibited the maximum value, which was about $9.1 \times 10^{-3}\ \Omega^{-1}\ cm^{-2}$. Then the $1/R_n$ of BM decreased rapidly. The decrease of $1/R_n$ lasted for about 1 h, then the $1/R_n$ of BM was almost constant around $4 \times 10^{-3}\ \Omega^{-1}\ cm^{-2}$. The variation of $1/R_n$ of BM indicated that the corrosion rate decreased firstly and then remained stable, which implied that the corrosion mechanism changed. The variation of $1/R_n$ of FGHAZ and ICHAZ was similar to that of BM, which indicated that similar corrosion processes occurred. The $1/R_n$ of CGHAZ also decreased rapidly and then approached a stable value (about $3 \times 10^{-3}\ \Omega^{-1}\ cm^{-2}$). However, there were some differences between CGHAZ and BM in the variation of $1/R_n$. Firstly, the falling period of $1/R_n$ of CGHAZ was longer than that of BM. Secondly, the $1/R_n$ of FGHAZ was at a slightly lower level than that of BM in the stable period, which meant that the corrosion rate of CGHAZ was lower than BM. It could be presumed that the corrosion process could be divided into two stages: stage one corresponded to the metastable pitting and stage two corresponded to the following pitting corrosion (BM, FGHAZ and ICHAZ) or uniform corrosion (CGHAZ).

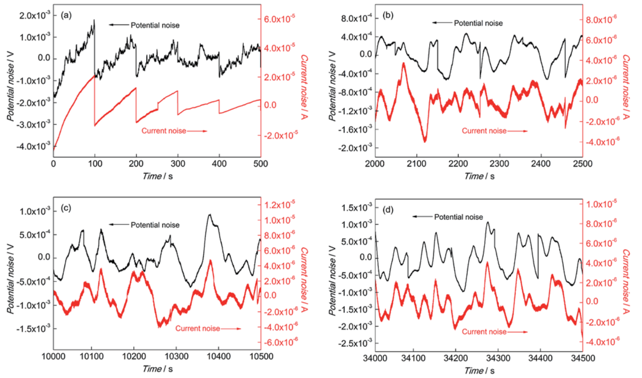

Fig. 4 EN records of FGHAZ during (a) 0–500 s, (b) 2000–2500 s, (c) 10 000–10 500 s and (d) 34 000–34 500 s in 0.1 mol L^{-1} HCl solution.

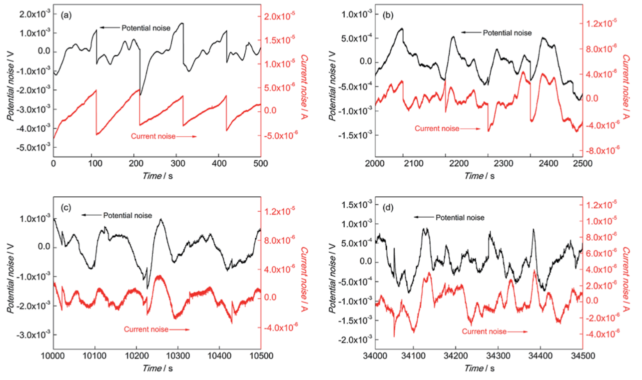

Fig. 5 EN records of ICHAZ during (a) 0–500 s, (b) 2000–2500 s, (c) 10 000–10 500 s and (d) 34 000–34 500 s in 0.1 mol L^{-1} HCl solution.

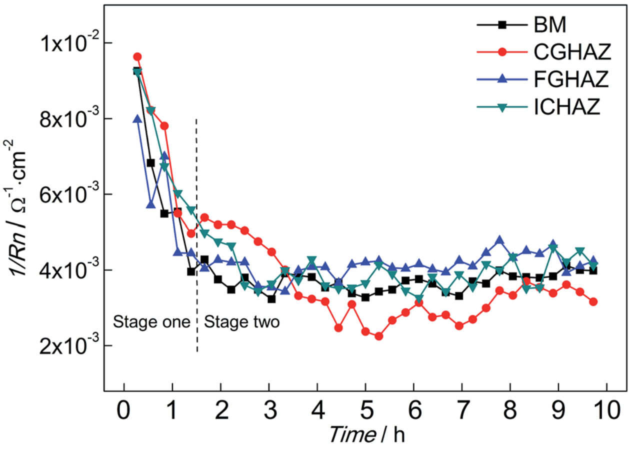

Fig. 6 Variations of $1/R_n$ of BM and simulated HAZ immersed in a 0.1 mol L^{-1} HCl solution.

3.3 Frequency domain analysis

As one of the most useful frequency domain analysis methods to EN data, the noise power spectral density (PSD) is able to reveal the corrosion mechanism of the electrode. The PSD can be obtained by fast Fourier transform (FFT) and the PSD of EPN is calculated as follows:[28]

$$\log \mathrm{PSD} = A + K \log f \tag{5}$$

where A and K are the noise intensity and the slope of straight-line region (high frequency section) of the PSD plots of EPN.

The parameters of the PSD plots including A and K are related to the corrosion process: the more positive the value of K indicates the greater probability to pitting corrosion; the higher the value of A represents more serious corrosion. In other words, the parameters of PSD plots have been proposed as indicators of the corrosion type and the corrosion rate.[29,30] The PSD plots of test electrodes after 10 h corrosion are shown in

Fig. 7 and the variations of PSD parameters of the test electrodes are shown in Fig. 8.

It can be found from Fig. 8 that the value of A of BM decreased slightly and then remained stable, which indicated that the corrosion strength of BM in the initial corrosion stage was the highest and then approached a stable level. In addition, the value of K of BM was steady with increasing time indicating that the probability of pitting corrosion on BM didn't change significantly. The parameters of the PSD plots of FGHAZ and ICHAZ were similar to that of BM, which indicated that the FGHAZ and ICHAZ underwent a similar corrosion process to BM.

On the CGHAZ electrode, the value of A of CGHAZ decreased firstly and then showed small fluctuations around a certain value, which indicated that the corrosion strength of CGHAZ approached stability after the decrease in the initial corrosion stage. Then K of CGHAZ fluctuated around a certain value. More importantly, the value of K of CGHAZ was smaller than that of BM, which meant that the probability of pitting corrosion of CGHAZ was lower than that of BM.

The indices including S_e and S_g were proposed by Zhang[31,32] to evaluate corrosion behavior and deduced by dimensional analysis of the PSD parameters. The indices S_e and S_g can be calculated according to the equations as follows:

$$S_e = f_c^{\,2}K^{1/2} \tag{6}$$

$$S_g = Wf_c^{\,-1}K^{-1} \tag{7}$$

where f_c is the cut-off frequency of the PSD plot, K is the slope of straight-line region and W is the constant value in the low frequency section of the PSD plot. It is reported that the value of S_e is positively related to the pitting corrosion strength and S_g characterizes the strength of the slow corrosion process (such as adsorption, diffusion, deposition and so on). In this paper, S_e and S_g were calculated from the PSD plots to reveal the corrosion process in detail.

Table 2 shows the PSD parameters of the test electrodes after different corrosion times while Fig. 9 shows the variations of S_e and S_g with time when immersed in a 0.1 mol L^{-1} HCl solution. It can be found that the S_e of the BM electrode decreased considerably firstly and then became stable. The variation of S_e for BM indicated that the pitting strength was the greatest at the beginning, then reduced and remained stable. Meanwhile, the S_g of the BM electrode increased in the first 1 h and then remained steady, which meant that the strength of the slow corrosion process increased in the initial corrosion stage. It could be implied that the pitting strength of CGHAZ reduced in the initial corrosion stage and then remained stable according to the variation of S_e of CGHAZ. However, the value of S_e for BM was higher than CGHAZ throughout the corrosion process, which meant that the pitting corrosion strength of BM was stronger. The S_g value of CGHAZ presented a larger fluctuation.

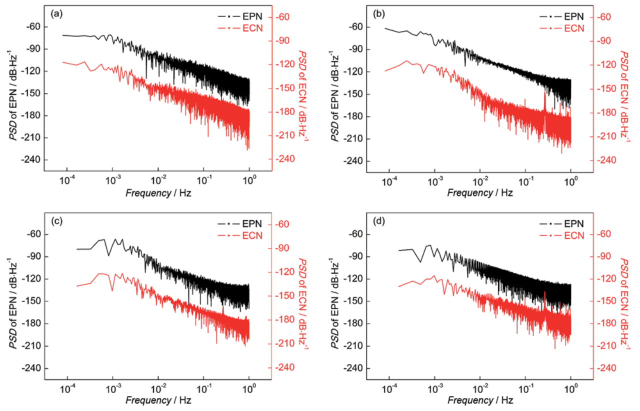

Fig. 7 PSD plots of (a) BM, (b) CGHAZ, (c) FGHAZ and (d) ICHAZ after 9 h corrosion in a 0.1 mol L^{-1} HCl solution.

Table 2 The PSD parameters of test electrodes in a 0.1 mol L^{-1} HCl solution after different corrosion times

Electrodes	Time (h)	f_c (dB/Hz)	K (dB/Hz^2)	W (dB/Hz)	S_g	S_e
BM	0	0.2034	19.92	59.80	0.1846	14.76
	3	0.1154	19.72	73.51	0.0591	32.31
	6	0.0978	19.52	73.01	0.0423	38.23
	9	0.0926	19.20	72.97	0.0376	41.06
CGHAZ	0	0.1259	21.00	55.56	0.0726	21.02
	3	0.0368	22.71	65.33	0.0065	78.14
	6	0.0477	21.46	61.91	0.0106	60.44
	9	0.0518	21.31	66.78	0.0124	60.51
FGHAZ	0	0.1656	19.61	75.99	0.1217	23.37
	3	0.1006	18.45	78.11	0.0434	42.10
	6	0.0972	18.56	76.78	0.0407	42.58
	9	0.0946	18.24	76.51	0.0383	44.32
ICHAZ	0	0.1942	19.43	83.34	0.1662	22.09
	3	0.1077	19.05	77.11	0.0507	37.56
	6	0.1210	18.04	79.40	0.0622	36.37
	9	0.0953	19.51	80.66	0.0401	43.40

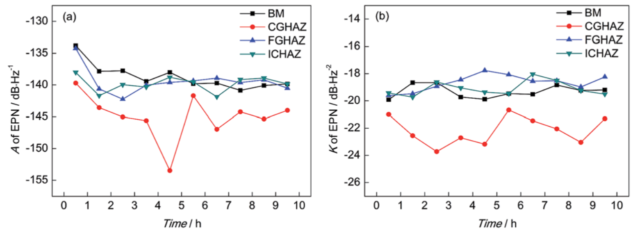

Fig. 8 Variations of (a) A and (b) K of test electrodes immersed in a 0.1 mol L^{-1} HCl solution.

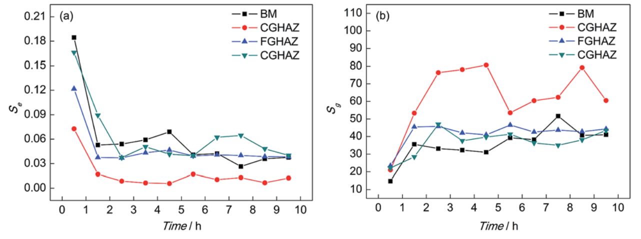

Fig. 9 Variations of (a) S_e and (b) S_g of test electrodes immersed in a 0.1 mol L^{-1} HCl solution.

Much of the instability seemed to result from the discontinuity of the adsorption and deposition. In addition, the value of S_g for CGHAZ was obviously higher than that of BM, which indicated that the strength of the slow corrosion process was greater than that of BM.

3.4 Wavelet transform

Wavelet transform (WT) is a mathematical method to discriminate and classify continuous signals and has been widely employed to analyze EN signals recently due to its ability to reveal information on the dominant corrosion process.[33,34] The independent corrosion events in the corrosion process are reflected by a series of wavelet energy, which contained the feature information about the time scale of the corrosion events: a smaller time scale of corrosion event corresponded to a faster corrosion process. Therefore, the greatest energy distribution in an energy distribution plot (EDP) represented the dominant corrosion events. In general, the energy distribution in crystals D1–D3, D4–D6 and D7–D8 reflects the corrosion information about the metastable pitting, pitting and slow frequency process when the crystals are ranged from D1 to D8.[35–38] For steel, the slow frequency process is usually related to oxygen diffusion and adsorption of hydrogen, which is an important feature of uniform corrosion. The EDPs of BM and the simulated HAZ specimens are shown in Fig. 10.

As shown in Fig. 10(a), it can be concluded that the wavelet energy was mainly dominated by the fast frequency energy (in the crystal D1) on the BM electrode at the beginning of corrosion, which meant that the metastable pitting mainly dominated the corrosion process of BM in this corrosion stage. About 0.5 h later, the wavelet energy was mainly accumulated in the crystals D4–D8, which might reflect the coexistence of the pitting corrosion and slow frequency process. It was indicated that the pitting and diffusion/adsorption occurred at the same time on the BM electrode. Fig. 10(b) shows the EDP of CGHAZ. It can be observed that the wavelet energy distribution was mainly accumulated in the crystal of D1 at the beginning and then changed into the crystals of D7–D8. It could be expected that the electrode surface of CGHAZ was mainly dominated by metastable pitting at the beginning and then turned into a slow frequency process. It could be demonstrated that the metastable pitting occurred on the surface of CGHAZ at first and then turned into uniform corrosion. FGHAZ and ICHAZ underwent a similar corrosion process to BM as indicated by the similar wavelet energy distribution to BM as shown in Fig. 10(c) and (d).

3.5 Potentiodynamic polarization and EIS

It has been reported that the EN technique is a very useful method to analyze the corrosion behavior, in particular when it is used in coordination with other electrochemical techniques such as potentiodynamic polarization, EIS and so on.[39–42] cathode polarization curves of all test electrodes, which indicated that all the electrodes underwent a similar cathodic polarization process. The anode current density decreased continuously with the increasing of potential, which Fig. 11 shows the potentiodynamic polarization curves of BM, CGHAZ, FGHAZ and ICHAZ in a 0.1 mol L^{-1} HCl solution. It can be seen that there were no significant differences in the reflected the active dissolution of electrode. All the anodic polarization curves showed no characteristics of passivation. However, the slope of anodic polarization curves of CGHAZ, FGHAZ and ICHAZ were bigger than that of BM, which implied that the welding thermal cycle affected the anodic polarization process.

The electrochemical parameters of the potentiodynamic polarization curves including corrosion potential E_{corr}, corrosion current density i_{corr}, anodic Tafel slopes β_a, cathodic Tafel slopes β_c and corrosion rate V are shown in Table 3, which were calculated by the Tafel Curve Fitting method proposed by Cao.[43] It can be found that the E_{corr} of CGHAZ was the lowest and the CGHAZ has the highest i_{corr}, while the E_{corr} and i_{corr} of the other electrodes were almost at the same level. This might be due to the difference in the anodic polarization process between CGHAZ and the others. The CGHAZ showed the lowest corrosion rate while the corrosion rate of the others were almost the same according to the electrochemical parameters as presented in Table 3.

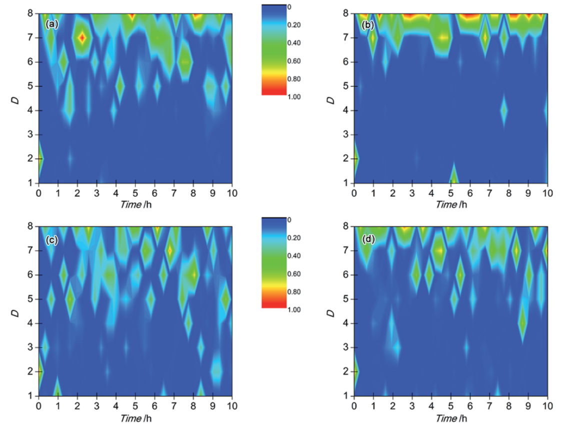

Fig. 10 EDPs of (a) BM, (b) CGHAZ, (c) FGHAZ and (d) ICHAZ immersed in a 0.1 mol L^{-1} HCl solution.

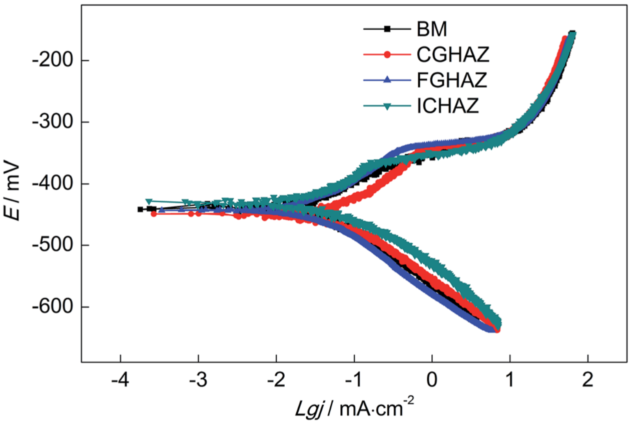

Fig. 11 The polarization curves of BM and simulated HAZ in a 0.1 mol L^{-1} HCl solution.

Table 3 Electrochemical parameters of polarization curves of test electrodes immersed in a 0.1 mol L^{-1} HCl solution

Electrodes	E_{corr} (mV)	i_{corr} (μA cm^{-2})	β_a (mV dec^{-1})	β_c (mV dec^{-1})	V (mm per year)
BM	−432	33.7	42.6	93.6	0.393
CGHAZ	−446	29.7	67.5	92.2	0.346
FGHAZ	−437	37.2	57.8	93.4	0.434
ICHAZ	−427	35.4	49.6	93.9	0.413

Fig. 12 shows the Nyquist plots of the test electrodes after different corrosion times in a 0.1 mol L^{-1} HCl solution. It can be observed that the Nyquist plots of all test electrodes showed one capacitive arc in a high frequency region, which suggested that the corrosion rate was mainly determined by the charge transfer process. The diameter of Nyquist plots of all test electrodes increased with increasing corrosion time, which implied that the corrosion resistance increased over time. In addition, the Nyquist plots of the CGHAZ electrode showed the greatest diameter, which meant that the corrosion resistance of CGHAZ was the greatest. The diameters of Nyquist plots of BM, FGHAZ and ICHAZ were almost at the same value indicating that corrosion resistance of these electrodes was nearly the same.

Fig. 13 shows the equivalent circuit to simulate the liquid/solid interface. R_{ct}, R_c and R_s represents the charge transfer resistance, the resistance to corrosion product and the solution resistance, respectively. C_c represented the corrosion product capacitance while the Constant Phase Element (CPE) referred to the double layer at the interface of the electrolyte and electrode.[44–47] Table 4 shows the parameters calculated by EIS based on the equivalent circuit as shown in Fig. 13. The R_{ct} of all the test electrodes was higher than R_c and R_s, which suggested that the corrosion processes of all test electrodes were mainly controlled by the charge transfer process in the 0.1 mol L^{-1} HCl solution.[47,48] The R_{ct} of all the test electrodes increased in the first 3 h and then showed no obvious change in the later corrosion stage, which meant the inhibiting effect on the charge transfer was enhanced in the initial corrosion stage and then became steady. It was implied that there might be differences in the corrosion process between the initial corrosion stage and later corrosion stage on the test electrodes. In addition, the R_{ct} of CGHAZ was larger than that of the other electrodes. It could be presumed that the CGHAZ electrode showed a larger charge transfer resistance than the other electrodes.

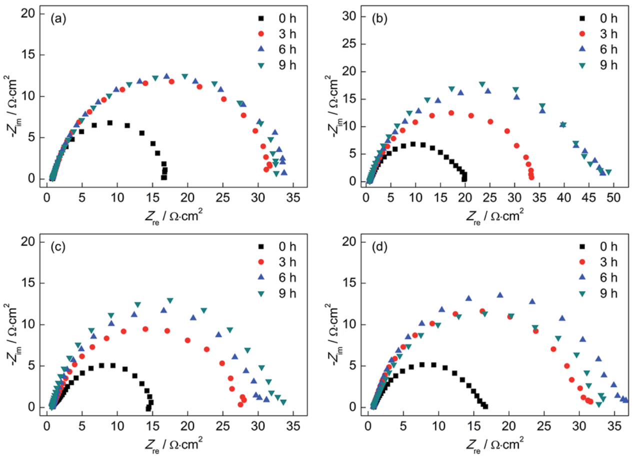

Fig. 12 Nyquist plots of (a) BM, (b) CGHAZ, (c) FGHAZ and (d) ICHAZ after different corrosion times in a 0.1 mol L^{-1} HCl solution.

3.6 Surface observation

Fig. 14 shows the SEM images of BM, CGHAZ, FGHAZ and ICHAZ of Q315NS. It can be observed from Fig. 14(a) that the BM of Q315NS mainly consisted of a polygonal ferrite (F) phase and pearlite (P) phase. The granular bainite (GB) with coarse grain boundaries could been found in the CGHAZ as shown in Fig. 14(b). The microstructure of GB consisted of bainitic ferrite matrix and the martensite/austenite phase (as the second phase).[49] Both FGHAZ and ICHAZ consisted of F and P. During the heating process of FGHAZ and ICHAZ, austenite transformation occurred when the HAZ was heated to A_{C1}. Then the austenite was transformed to F and P in the cooling process, which resulted in the microstructure of FGHAZ and ICHAZ as shown in Fig. 14(c) and (d).

It could be found that the grain size of CGHAZ was larger than that of BM, FGHAZ and ICHAZ. Usually the austenite grain size increases with peak temperature because the higher temperature will bring about a larger diffusion rate.[50] As a result, the CGHAZ had the largest grain size due to the highest peak temperature. The grain of FGHAZ was further refined due to the fast cooling rate when the austenite transformed to F and P. Thus, the grain size of FGHAZ was smaller than that of BM while the grain size of ICHAZ was similar to that of BM.

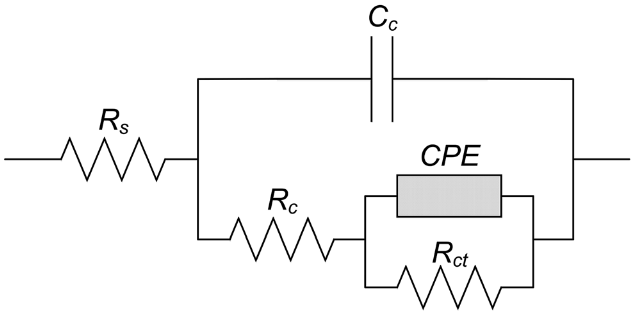

Fig. 13 Equivalent circuit for EIS.

Table 4 Electrochemical parameters of EIS of test electrodes immersed in a 0.1 mol L^{-1} HCl solution

					CPE		
Electrodes	Corrosion time (h)	R_s (Ω cm^2)	C_c (μF)	R_c (Ω cm^2)	Y (S s^n cm^{-2})	N	R_{ct} (Ω cm^2)
BM	0	0.7942	417.1	0.5753	1.464×10^{-3}	0.823	15.66
	3	0.8181	124.6	0.5760	1.001×10^{-3}	0.777	30.88
	6	0.7327	137.3	0.4751	1.254×10^{-3}	0.748	34.50
	9	0.7998	178.2	0.8595	1.313×10^{-3}	0.753	32.66
CGHAZ	0	0.7050	147.7	0.9751	1.514×10^{-3}	0.736	18.16
	3	0.7323	136.7	0.4779	1.218×10^{-3}	0.753	33.85
	6	0.6848	139.1	0.9208	1.153×10^{-3}	0.737	45.68
	9	0.6948	138.1	1.0192	1.010×10^{-3}	0.752	44.92
FGHAZ	0	0.8594	193.2	1.1869	3.245×10^{-3}	0.787	12.96
	3	0.8450	161.3	0.9572	1.574×10^{-3}	0.754	25.44
	6	0.8025	265.3	1.0612	1.349×10^{-3}	0.788	27.78
	9	0.6889	312.1	0.9087	1.015×10^{-3}	0.811	29.85
ICHAZ	0	0.8095	225.4	0.8838	3.045×10^{-3}	0.713	14.64
	3	0.7528	195.7	1.0755	1.055×10^{-3}	0.776	29.19
	6	0.7506	168.2	1.2441	9.078×10^{-4}	0.776	33.95
	9	0.7614	132.9	1.1039	1.349×10^{-3}	0.749	31.45

The SEM images of BM and simulated HAZ after 10 h corrosion in a 0.1 mol L^{-1} HCl solution are shown in Fig. 15. It can be found that some pits appeared mainly on the pearlite region of BM as shown in Fig. 15(a), which demonstrated that the pitting corrosion occurred. However, there were no obvious pits on the ferrite region, which might be because the pearlite was corroded prior to this. Eventually, the pitting corrosion mainly occurred on the pearlite region of BM. The FGHAZ and ICHAZ seemed to undergo the similar corrosion process to BM according to the similar corrosion morphologies, which are shown in Fig. 15(c) and (d), respectively. As shown in Fig. 15(b), there were no obvious pits formed on the surface of CGHAZ, which showed typical uniform corrosion. This might be due to the homogeneity of the microstructure of CGHAZ. There was no obvious oxide film formed on the surface of all test electrodes, which indicated that no passivation occurred. From the surface corrosion morphology of the test electrodes as shown in Fig. 15, we arrived at the conclusion that pitting corrosion occurred at BM, FGHAZ and ICHAZ, while CGHAZ was mainly dominated by uniform corrosion.

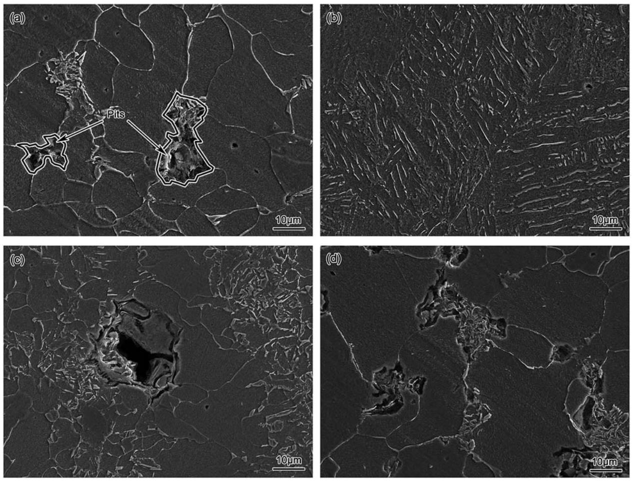

Fig. 15 SEM images of (a) BM, (b) CGHAZ, (c) FGHAZ and (d) ICHAZ after 10 h corrosion in a 0.1 mol L^{-1} HCl solution.

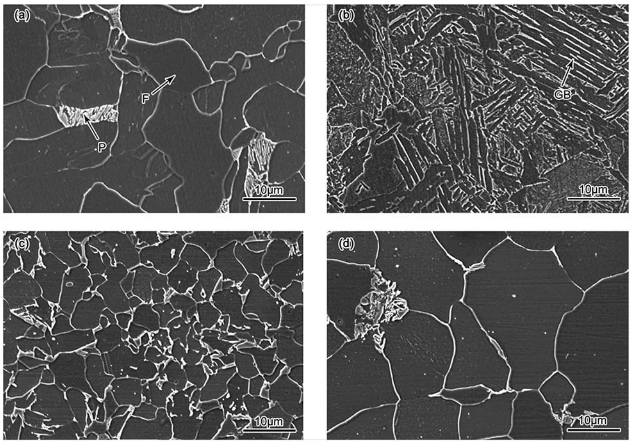

Fig. 14 SEM images of (a) BM, (b) CGHAZ, (c) FGHAZ and (d) ICHAZ.

4 Conclusion

The corrosion processes of BM and the simulated HAZ of Q315NS steel in a 0.1 mol L^{-1} HCl solution at 60 °C were investigated by EN, potentiodynamic polarization, EIS and surface observation. The main conclusions are as follows:

(1) The corrosion process of BM of Q315NS could be divided into two stages: the initial metastable pitting stage and the following pitting corrosion stage. The pitting corrosion was owing to the existence of pearlite which was corroded previously. The FGHAZ and ICHAZ of Q315NS showed nearly the same corrosion process as BM due to the similar microstructure.

(2) Two corrosion stages could be clearly distinguished as the initial metastable pitting stage and the uniform corrosion stage in the corrosion process of CGHAZ. The corrosion process of CGHAZ was mainly dominated by oxygen diffusion and adsorption of hydrogen in the uniform corrosion stage.

(3) With increasing time, the corrosion strength of BM, CGHAZ, FGHAZ and ICHAZ of Q315NS remained constant after a significant decrease. The corrosion rate of CGHAZ was slightly lower than that of the other electrodes, and there was no obvious difference in the corrosion rate among BM, FGHAZ and ICHAZ.

Conflicts of interest

There are no conflicts to declare.

Acknowledgements

The authors are grateful for the financial support of the Natural Scientific Research Innovation Foundation in the Harbin Institute of Technology (No. HIT.NSRIF.201703) and the Shandong Provincial Natural Science Foundation of China (No. ZR2016EEQ03).

References

1 Y. G. Yang, T. Zhang, Y. W. Shao, G. Z. Meng and F. H. Wang, *Corros. Sci.*, 2013, **71**, 62–71.
2 D. P. Le, W. S. Ji, J. G. Kim, K. J. Jeong and S. H. Lee, *Corros. Sci.*, 2008, **50**, 1195–1204.
3 W. Zhang, Y. P. Ma and Y. G. Liu, *Anhui Metall.*, 2009, **3**, 25–27.
4 I. Matsushima, *Low Alloy Corrosion Resistant Steel-A History of Development Application and Research*, Metallurgical Industry Press, Beijing, 2004.
5 X. X. Ye, C. Zhou and C. Zhang, *Corros. Sci. Prot. Technol.*, 2015, **27**, 135–140.
6 Y. H. Qian, Z. G. Li and A. N. Yang, *Spec. Steel*, 2005, **26**, 30–34.
7 Z. Y. Liang and Q. X. Zhao, *Eng. Failure Anal.*, 2013, **28**, 208–214.
8 H. Cai, *Ind. Boil.*, 2005, **5**, 22–25.
9 J. Verma and R. V. Taiwade, *J. Manuf. Process*, 2016, **14**, 1–10.
10 J. S. Wei, Y. C. Qi, Z. L. Tian and Y. Peng, *J. Iron Steel Res. Int.*, 2016, **23**, 955–962.
11 L. J. Dong, Q. J. Peng, E. H. Han, W. Ke and L. Wang, *Corros. Sci.*, 2016, **107**, 172–181.
12 H. L. Ming, Z. M. Zhang, P. Y. Xiu, J. Q. Wang, E. H. Han, W. Ke and M. X. Su, *Acta Metall. Sin.*, 2016, **26**, 848–858.
13 S. R. Reza, *Opt. Laser Technol.*, 2016, **82**, 113–120.
14 S. Q. Zhang, H. Y. Zhao, F. Y. Shu, W. X. He and G. D. Wang, *Metals*, 2017, **7**, 194–206.
15 X. H. Yu, J. L. Caron, S. S. Babu, J. C. Lippold, D. Isheim and D. N. Seidman, *Acta Mater.*, 2010, **58**, 5596–5609.
16 J. Hu, L. X. Du, H. Xie, F. T. Dong and R. D. K. Misra, *Mater. Des.*, 2014, **60**, 302–309.
17 Y. Y. Wang, R. Kannan and L. J. Li, *Mater. Charact.*, 2016, **118**, 225–234.
18 F. Hayat and H. Uzun, *J. Iron Steel Res. Int.*, 2011, **18**, 65–72.
19 W. Y. Zhang, *Welding Metallurgy (Basic Principle)*, China Machine Press, Beijing, 2014.
20 R. A. Cottis, *Corrosion*, 2001, **57**, 265–285.
21 W. Liu, G. W. Sun, C. B. Li, X. F. Li, R. Liu, Q. Qiu and W. Yang, *Corros. Prot.*, 2016, **37**, 609–612.
22 Y. J. Tan, S. Bailey and B. Kinsella, *Corros. Sci.*, 1996, **38**, 1681–1695.
23 F. Mansfeld, Z. Sun and C. H. Hsu, *Electrochim. Acta*, 2001, **46**, 3651–3664.
24 U. Bertocci, F. Huet, P. Rousseau and R. P. Nogueira, *Corrosion*, 2002, **58**, 337–347.
25 Y. F. Cheng, M. Wilmott and J. L. Luo, *Corros. Sci.*, 1999, **41**, 1245–1256.
26 M. J. Bahrami, M. Shahidi and S. M. A. Hosseini, *Electrochim. Acta*, 2014, **148**, 127–144.
27 J. F. Chen and W. F. Bogaerts, *Corros. Sci.*, 1995, **37**, 1839–1842.
28 L. Liu, Y. Li and F. H. Wang, *Electrochim. Acta*, 2008, **54**, 768–780.
29 Y. F. Cheng, B. R. Rairdan and J. L. Luo, *J. Appl. Electrochem.*, 1998, **28**, 1371–1375.
30 Z. Zhang, J. Q. Zhang, J. M. Wang and N. C. Chu, *Chin. J. of Nonferrous Met.*, 2001, **11**, 284–287.
31 Y. Y. Shi, Z. Zhang, F. H. Cao and J. Q. Zhang, *Electrochim. Acta*, 2008, **53**, 2688–26987.
32 Z. Zhang, J. Q. Zhang, J. F. Li, J. M. Wang and C. N. Cao, *Acta Phys.-Chim. Sin.*, 2001, **17**, 651–654.
33 A. Aballe, M. Bethencourt, F. J. Botana and M. Marcos, *Electrochim. Acta*, 1999, **44**, 4805–4816.
34 P. Planinsic and A. Petek, *Electrochim. Acta*, 2008, **53**, 5206–5214.
35 A. M. Homborg, T. Tinga, X. Zhang, E. P. M. V. Westing, P. J. Oonincx, G. M. Ferrari, J. H. W. D. Wit and J. M. C. Mol, *Electrochim. Acta*, 2013, **104**, 84–93.
36 M. J. Bahrami, M. Shahidi and S. M. A. Hosseini, *Electrochim. Acta*, 2014, **148**, 127–144.
37 F. H. Cao, Z. Zhang, J. X. Su, Y. Y. Shi and J. Q. Zhang, *Electrochim. Acta*, 2006, **51**, 1359–1364.
38 L. J. Zhang, Z. Zhang and J. Q. Zhang, *Acta Phys.-Chim. Sin.*, 2008, **24**, 1831–1838.
39 H. A. Sorkhabi, D. Seifzadeh and M. R. Boroujeni, *Arabian J. Chem.*, 2016, **9**, S1320–S1327.
40 J. Mojica, E. García, F. J. Rodríguez and J. Genescá, *Prog. Org. Coat.*, 2001, **42**, 218–225.
41 M. G. Pujar, N. Parvathavarthini, R. K. Dayal and S. Thirunavukkarasu, *Corros. Sci.*, 2009, **51**, 1707–1713.
42 A. Ehsani, M. G. Mahjani, M. Hosseini, R. Safaria, R. Moshrefi and H. M. Shiri, *J. Colloid Interface Sci.*, 2017, **490**, 444–451.
43 C. N. Cao, *Principles of Electrochemistry of Corrosion*, Chemical Industry Press, Beijing, 3rd edn, 2008.
44 X. X. Wang, Y. M. Gao, K. Li, J. B. Yan, Y. F. Li and J. B. Feng, *Corros. Sci.*, 2013, **69**, 369–375.

45 X. X. Wang, Y. M. Gao, Y. F. Li and T. Yang, *Corros. Sci.*, 2014, **87**, 211–217.

46 K. Jüttner, *Electrochim. Acta*, 1990, **35**, 1501–1508.

47 Q. B. Zhang and Y. X. Hua, *Electrochim. Acta*, 2009, **54**, 1881–1887.

48 M. E. Achouri, S. Kertit, H. M. Gouttaya, B. Nciri, Y. Bensouda, L. Perez, M. R. Infante and K. Elkacemi, *Prog. Org. Coat.*, 2001, **43**, 267–273.

49 Z. Q. Cui and B. X. Liu, *Metallurgy and Treatment Theory*, Harbin Institute of Technology Press, Harbin, 3rd edn, 2007.

50 J. Moon, J. Lee and C. Lee, *Mater. Sci. Eng., A*, 2007, **459**, 40–46.